Reaction Chemistry & Engineering

ROYAL SOCIETY OF CHEMISTRY

PAPER

View Article Online
View Journal

Cite this: DOI: 10.1039/d5re00442j

Mechanistic insights into the thermal pyrolysis of high-density polyethylene and polypropylene: towards sustainable hydrogen production and carbon valorization

Vanessa Maria Pohl, † Cedric Karel Fonzeu Monguen, † Dominik Julian Heitlinger, Patrick Lott * and Olaf Deutschmann

High-temperature pyrolysis of plastic waste presents a viable approach for concurrent hydrogen production and carbon material synthesis, contributing to energy recovery and environmental remediation. This study investigates the pyrolysis behavior of high-density polyethylene (HDPE), polypropylene (PP), and their mixtures in a high-temperature laboratory-scale reactor across a temperature range of 700 °C to 1600 °C. The objective was to assess how polymer composition and temperature influence the distribution of gaseous, liquid, and solid products. Gas phase analysis revealed a strong temperature dependence in hydrogen and hydrocarbon yields, with distinct variations between individual polymers and their mixtures. This underscores the relevance of investigating the pyrolysis of mixtures, as plastic wastes typically contain multiple polymer materials. Liquid products, primarily hydrocarbons, exhibited increased aromaticity and decreased yields at higher temperatures, indicating enhanced secondary cracking. Solid carbonaceous residues were characterized using Raman spectroscopy and X-ray diffraction (XRD). Raman spectroscopy revealed a decline in graphitization degree with increasing temperature, suggesting higher defect density and reduced structural (graphitic) ordering. Conversely, XRD data demonstrated increased crystallite sizes and decreased interlayer spacing with temperature, implying the formation of more ordered crystalline domains. PP pyrolysis resulted in carbon with the highest graphitization degree and crystallinity at moderate temperatures. The HDPE/PP mixture exhibited a synergistic effect that improves graphitic ordering and crystallite growth, surpassing the simple average of the pure components, particularly between 1200 °C and 1400 °C. At 1600 °C, thermal effects dominate, minimizing the influence of specific polymers and leading to converge all samples toward similar carbon structural characteristics. These findings underscore the critical role of polymer composition and temperature in optimizing pyrolysis processes for thermochemical hydrogen generation and carbon capture from mixed plastic waste.

Received 29th September 2025,
Accepted 28th January 2026

DOI: 10.1039/d5re00442j

rsc.li/reaction-engineering

Introduction

The significant increase in plastic production, which meanwhile exceeds 400 Mt annually,[1] makes the effective management of plastic waste (PW) increasingly critical. Improper disposal of PW greatly contributes to marine pollution and the formation of microplastics. Given that a substantial portion of PW is discarded rather than recycled, the main goal of waste management should be PW valorization. Polyethylene (PE), which includes low-density polyethylene (LDPE) and high-density polyethylene (HDPE), is the most extensively produced and consumed plastic worldwide, accounting for approximately 32% of the total municipal solid waste.[2] HDPE, a thermoplastic characterized by its excellent strength-to-density ratio, is commonly used in the production of containers for cleaning agents, as well as food and beverage packaging.[3] Polypropylene (PP) represents approximately 11–18% of the total PW generated worldwide and is recognized as the most prevalent thermoplastic.[4,5] Its simple molecular structure, consisting of a linear chain of carbon atoms with periodic methyl group substitutions, imparts resistance to chemical degradation and thermal stress. These properties render PP highly suitable for a variety of functional and consumer products, ranging from flexible barrier film bags for food packaging to stackable crates for industrial transport and storage.[6]

Institute for Chemical Technology and Polymer Chemistry (ITCP), Karlsruhe Institute of Technology (KIT), Engesserstr. 20, 76131 Karlsruhe, Germany.
E-mail: patrick.lott@kit.edu
† Both contributed equally.

In the European Union, the landfilling of PW is strongly discouraged due to its environmental impact.[7] To date, the most effective treatment method is energy recovery through incineration, which removes PW from the economic cycle. In contrast, direct recycling reintroduces plastic waste into the value chain, but this process is often uneconomical due to the need for pre-sorting. Additionally, the complexity of packaging materials, which frequently consist of various types of plastic, complicates the recycling process and increases operational costs.

Thermal pyrolysis offers a promising solution for the thermochemical treatment of mixed plastic waste streams.[8] At temperatures exceeding 800 °C, pyrolysis predominantly yields hydrogen and solid carbon, both of which are critical feedstocks for the chemical industry.[9] This process provides an opportunity to reduce the carbon footprint of chemical production by using the byproducts of plastic pyrolysis. For instance, hydrogen is commonly produced through steam reforming, which is associated with substantial CO_2 emissions. Although water electrolysis provides a cleaner alternative, it requires a high energy input of 286 kJ mol^{-1}. Therefore, the thermal pyrolysis of plastic waste emerges as a more energy-efficient and CO_2-free route for hydrogen generation, while simultaneously addressing plastic waste management.

Given the compositional diversity of post-consumer PW, this study investigates the pyrolysis behavior of HDPE and PP individually, followed by experiments with a 1 : 1 weight ratio mixture of these plastics to simulate realistic plastic waste streams. The mixture of two plastic types mimics more realistic conditions of real-life plastic waste which is commonly a mixture of various plastics. Their simultaneous copyrolysis would avoid the need for mechanical separation, herewith saving several process steps. By combining online gas phase analysis, analysis of the liquid phase, and characterization of the solid carbon accruing during pyrolysis, this study assesses how polymer composition and temperature influence the distribution of gaseous, liquid, and solid products. In contrast to several previous studies that investigated plastics pyrolysis with the aim of producing pyrolysis oil at lower temperatures, occasionally employing catalytic materials,[10–12] the present work focuses on entirely thermal and as complete as possible pyrolysis at temperatures of up to 1600 °C. This approach facilitates the production of the C-free energy carrier hydrogen and solid carbon materials that may be re-used, *e.g.*, in the rubber industry.

Experimental

Materials

Commercially available high-density polyethylene, denoted HDPE (linear formula: $H(CH_2CH_2)_nH$, product number 547999), and polypropylene, denoted PP (linear formula: $[CH_2CH(CH_3)]_n$, product number 428116), were obtained from Sigma-Aldrich (affiliate of Merck KGaA, Darmstadt, Germany) in pellet form with a granule size of 5 mm, smooth surface morphology, and a minimum layer thickness of 0.11 mm. The HDPE sample exhibited a melt index of 0.22 g min^{-1} (190 °C/2.16 kg) and a transition temperature of 123 °C. The PP sample was characterized by a number-average molecular weight (M_n) of ~5000 and a weight-average molecular weight (M_w) of ~250 000; furthermore, it had a density of 0.9 g mL^{-1}, a melting point of 157 °C, and a transition temperature of 163 °C.

Carbon material characterization

The structural analysis of carbonaceous pyrolysis residues was conducted using Raman spectroscopy and X-ray diffraction (XRD). Raman spectra were acquired using an inVia Reflex spectrometer (Renishaw), equipped with a He–Ne laser operating at 633 nm and a power of 17 mW. A diffraction grating with 600 gr mm^{-1} was used. X-ray diffraction (XRD) measurements were conducted using a PANalytical X'pert PRO diffractometer (Malvern PANalytical). The carbon samples were analyzed over a range of 2θ angles from 5.0° to 80.0° under Cu-K-α radiation, with the Cu-K-β component filtered out using a nickel filter. Consistent with values reported in the literature for disordered carbon materials,[13] a shape factor (K) of 0.89 was applied in order to estimate the crystallite size D of the carbon structures using the Debye–Scherrer equation (eqn (1)) on the peak with the highest intensity:

$$D = 0.9\lambda/\beta\cos\theta \quad (1)$$

where β is the diffraction broadening on the peak at half-height for Bragg's angle θ, and λ represents the wavelength of the X-ray radiation.

Experimental reactor setup

Experiments were conducted in a laboratory-scale, high-temperature reactor under pressure conditions ranging from 1 to 4 bar and temperatures between 700 °C to 1600 °C, with argon used as the inert gas. The experimental setup that is schematically depicted in Fig. 1 and that has been described in greater detail in previous publications[14–16] includes several components. Gases are dosed *via* mass flow controllers (Bronkhorst) and fed from the top of the reactor. The actual tubular reactor is made of ceramic α-Al_2O_3 (DEGUSSIT AL23 by Friatec/Aliaxis), has an inner diameter of 20 mm and a length of 1000 mm. Heating rods maintain the required temperature and create an isothermal zone of approx. 400 mm length. Representative axially resolved temperature profiles within the reactor are illustrated in Fig. S5 for temperatures ranging from 1000 to 1600 °C. These temperature profiles, which match those available from previous publications of our group employing the same setup[17] clearly depict the isothermal hot zone. A flange and filter system are positioned at the bottom and downstream, respectively, to collect the carbon produced during the

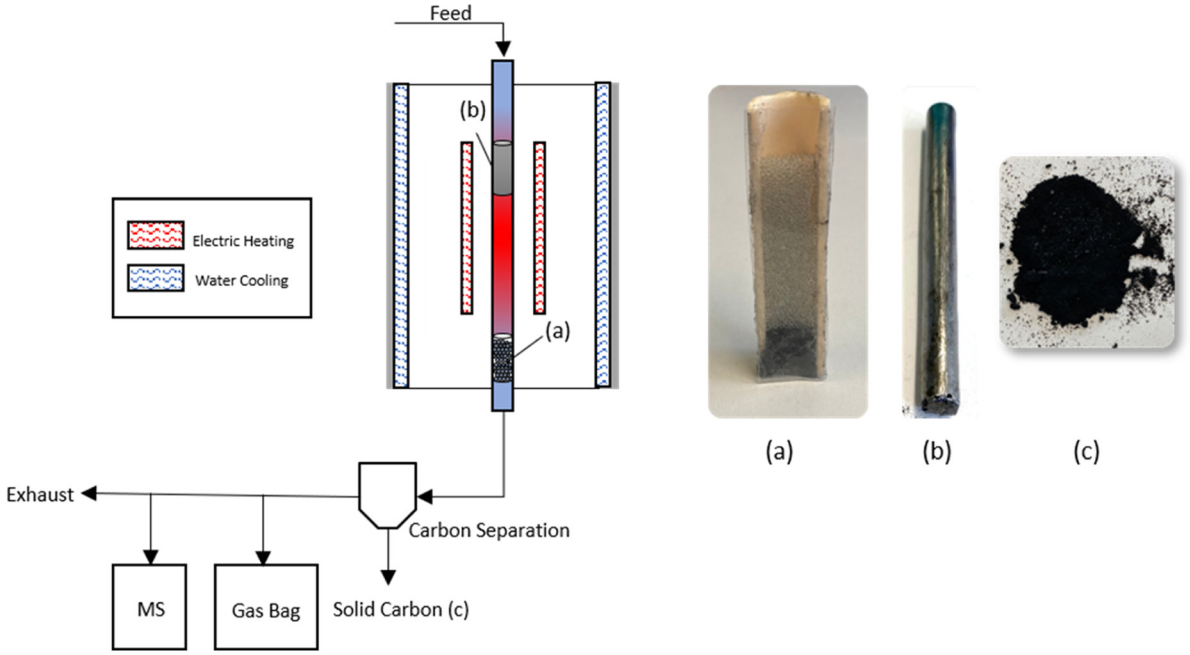

Fig. 1 Scheme of the experimental setup used for the plastic pyrolysis experiments in this work. (a) Glass pearl bed placed downstream to collect condensed liquids, (b) graphite container positioned at the beginning of the isothermal zone, and (c) carbon.

reaction. Reactor operation parameters such as temperature and gas flow rate are precisely controlled and monitored using a LabVIEW software tool. A solid dosing unit is employed to purge the plastic samples with argon and to subsequently introduce them into the reactor. A graphite container that was placed at the beginning of the isothermal zone and whose weight was recorded prior to mounting in the reactor, contained the plastic sample and kept it in place during the pyrolysis experiment.

At the end of the reaction pipe, a bed of glass pearls (pearl diameter: 1 mm) was installed in a ceramic container to facilitate the condensation of aliphatic and polyaromatic hydrocarbons forming during the reaction. The product gases are collected in a gas bag and subsequently analyzed using a gas chromatography (GC) device (Agilent, model 6890 N) equipped with a HAYESEP model Q 100/120 column; helium served as carrier gas.

Product analysis

For each experiment, 0.3 g of plastic pellets were purged with argon in the dosing unit at a flow rate of 100 mL min^{-1}. During the reaction, the argon gas flow was set to provide a residence time of 10 s in the isothermal hot zone; during initial screening experiments (see SI), this was determined to keep balance between adequate dilution and sufficient reaction times. The specific flow rates for the different temperatures are provided in the SI (Table S3).

The purging chamber was connected to a ball valve, allowing the polymer to be dosed directly into the reaction tube, where it fell into the graphite container. The gas evolving during the pyrolysis experiment was collected in a gas bag and later analyzed by means of GC, which allowed for the detection of argon, methane, ethane, ethylene, acetylene, and propylene with a thermal conductivity detector (TCD). The GC was calibrated accordingly to check the amount H_2 that is measured. For the GC-calibration, we utilized one gas bottle containing H_2 and C_1 to C_3 species to calibrate the C_1 to C_3 range. Another gas bottle, which contained a mixture of H_2, Ar, and CH_4, was used to calibrate Ar. The GC signals were evaluated by data integration. To quantify hydrogen, a known amount was simultaneously dosed into the gas chromatograph at a concentration of 10%, ensuring accurate chromatography results. This procedure was necessary because the TCD exhibits limited sensitivity toward low hydrogen concentrations, requiring calibration at elevated H_2 levels to ensure a linear and reliable detector response. Note that the GC was always calibrated prior to the experiments and each experiment was repeated three times to ensure reproducibility. The average value from three experiments was taken. The standard deviation in regard of the gas phase species is less than 5%.

In the experiments used for gas- and liquid-phase evaluation, the amount of carbon formed was too low for solid phase characterization. Therefore, plastic was added in consecutive experimental runs. While the setup configuration for generating carbon samples for analysis and characterization was the same as described above in principle, the glass pearl bed was removed and instead a cyclone wand and filter were used to separate the produced carbon from the gas stream. This circumvents an undesired increase in backpressure that would have occurred during consecutive runs due to carbon accumulation in the glass pearl bed.

For the carbon-collection experiments, a total of 15 consecutive pyrolysis runs were carried out for each temperature. In each run, 0.3 g of plastic was introduced into the reactor. Once the mass spectrometer (MS) indicated completion of the reaction, the next 0.3 g portion was added. In total, 4.5 g of plastic were processed at one reaction condition. The cumulated mass of solid carbon recovered after all 15 runs ranged from 0.8 to 1.3 g, depending on temperature, with higher temperatures yielding larger amounts of solid carbon. Note that this absolute number may be heavily influenced by experimental and human error, as carbon can also deposit in pipes and reactor walls, and the carbon from the filter system is collected manually.

Samples of the liquid condensable product phase were systematically collected from different sites, including the flange of the reactor outlet, the downstream cyclone, the fine filters placed along the pipeline going to the analyzers, and the connection between product lines. To ensure comprehensive collection, soot accumulated in all devices was removed. Each device was then flushed with *n*-hexane, wiped with filter paper, and further cleaned using ultrasonic treatment. The collected soot and filter papers underwent a solvent extraction process in a Soxhlet equipment for 4 hours, utilizing *n*-hexane as the extraction solvent.

The Soxhlet extract was subjected to solid phase extraction (SPE) for separating aliphatic and polycyclic aromatic hydrocarbons (PAHs) employing UCT Enviro-Clean Fusion Ag^+ sorbent, which features silver ions functionalized on a solid framework. PAHs are effectively maintained on the sorbent through the formation of a charge-transfer combination with ionized silver. This process implies a high capacity for PAHs, preventing any breakthrough into the aliphatic fraction. The nonpolar solvent hexane is then used to flush the aliphatic species *via* a stationary state without being retained, while the PAHs remain adsorbed. To desorb the PAHs, the polar solvent acetone is applied. Consequently, two fractions – aliphatic and PAHs – are collected and analyzed using GC. The GC device used is a ThermoFischer Scientific Trace 1310 GC, equipped with a J&W Scientific DB-5 MS column (25 m × 0.32 mm, d_f = 0.25 μm). The two SPE fractions are introduced into the GC and analyzed separately. The different elements are differentiated utilizing a temperature schedule that begins at 40 °C. After 2 minutes, the temperature rises to 120 °C at a rate of 30 °C min^{-1}, and subsequently with 8 °C min^{-1} until it reaches 330 °C.

To calculate the yields of the distinct species present in the gas phase, the GC findings were examined according to the following procedure: beginning with the averaged findings from the three GC analyses, the volume fractions were processed into the yield of the respective species. This conversion method involved calculating the dosed argon volume over the entire experiment duration employing the reactor's measurement file. The overall volume $V_{T_{gb}}$ of the gas bag was then evaluated by combining the argon volume fraction y_{Ar}^{GC} with the dosed argon volume V_{Ar}, as outlined in eqn (2). The dosed argon volume was determined by multiplying the argon gas flow rate by the reaction time, with a flow rate of 175 mL min^{-1} for a gas residence time of 10 s at 1000 °C.

$$V_{T_{gb}} = V_{Ar}/y_{Ar}^{GC} \quad (2)$$

The respective quantity of component n_j of the species CH_4, CO, CO_2, C_2H_2, C_2H_4, C_2H_6, and C_3H_6 is calculated using eqn (3).

$$n_j = y_j^{GC}(pV_{T_{gb}}/RT) \quad (3)$$

where p is the ambient pressure, R is the ideal gas constant and T is the ambient temperature.

The amount of hydrogen is determined by balancing the quantity of the analyzed substance. This involves subtracting the sum of the amount of substance of all product gas species n_i from the overall quantity of component in the sample bag, as shown in eqn (4).

$$n_{H_2} = (pV_{T_{gb}}/RT) - \sum n_{iexcl.H_2} \quad (4)$$

With the initial weight of the polymer $m_{Polymer}$ and the specific molar mass M_i of each species, the yield Y_i per gram of polymer can be calculated using eqn (5). The fraction of the sum of all gaseous product masses and the polymer mass provides the gas yield in eqn (6).

$$Y_i = (n_i M_i/m_{Polymer}) \quad (5)$$

$$Y_{Gas} = \sum(n_i M_i)/m_{Polymer} \quad (6)$$

The total yield of solid and condensable phases is expressed by the relationship in eqn (7).

$$Rest_{solid+condesed\ phase} = 1 - Y_{Gas} \quad (7)$$

The yields of the individual fractions of the liquid phase were evaluated using eqn (8). In this context, $m_{i,liq}$ represents the mass of a specific fraction of the liquid phase, as analyzed by GC. Further details on the GC analysis of the liquid sample can be found in Tables S1 and S2 in the SI.

$$Y_{i,liq} = m_{i,liq}/m_{Polymer} \quad (8)$$

Results and discussion

Influence of temperature on the gas phase species evolving from HDPE pyrolysis

A pressure peak was observed for all reactions after the polymer was introduced into the reactor, with the peak

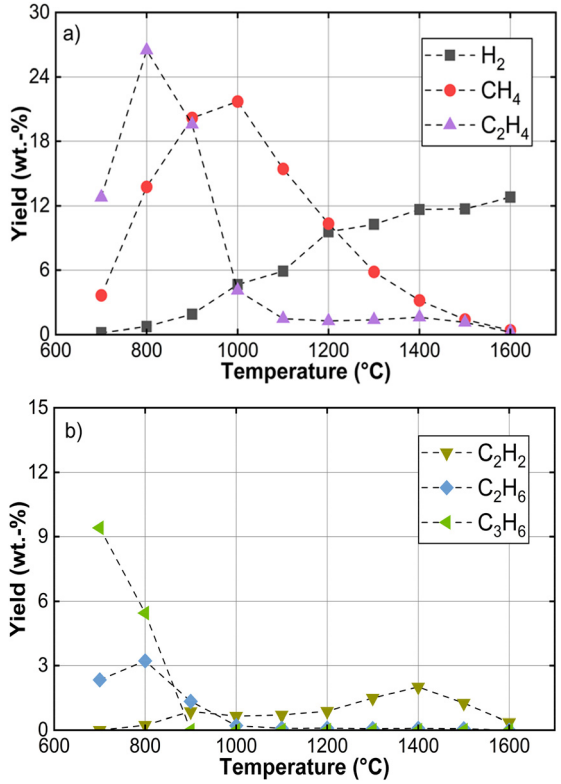

Fig. 2 Gas phase results of the HDPE pyrolysis with τ = 10 s at 1 bar. Temperature variation from 700 °C to 1600 °C with yields of main (a) and minor (b) gaseous products.

becoming more pronounced at higher temperatures. The pressure consistently returned to the target pressure within a few seconds, indicating that the main part of the reaction was completed during this brief period. The effect of pressure is discussed in greater detail later. As illustrated in Fig. 2 the temperature was varied between 700 °C and 1600 °C in a first set of experiments while keeping the pressure constant at 1 bar.

At 700 °C and 800 °C, ethylene (C_2H_4) is the primary reaction product, before the pyrolysis of HDPE results predominantly in methane (CH_4) formation at temperatures of 900–1200 °C. Even higher temperatures maximize the yield of hydrogen, which is the target product. Therefore, in our case the optimum temperature for mere high hydrogen yield would be 1600 °C. However, since also other factors such as carbon quality and energy demand need to be considered, defining an optimum temperature for the overall process is much more complex. The formation of ethane (C_2H_6) and propylene (C_3H_6) is relevant only at low temperatures and becomes negligible at 1000 °C and above, whereas acetylene (C_2H_2) formation appears to be relevant over a broad temperature range from 900 °C to 1500 °C. These product yield trends can be explained under consideration of the underlying HDPE decomposition mechanism. First, the polymer chains decompose during thermal cracking reactions that primarily yield the monomer molecule, namely ethylene. As the temperature increases, the relevance of dehydrogenation reactions yielding elemental hydrogen increases, however, apparently also resulting in methane formation. Thermodynamic considerations as well as mechanistic investigations on hydrocarbon pyrolysis suggest that the recombination of methyl (CH_3) radicals with hydrogen atoms can result in CH_4 formation if the temperature is insufficient to allow for complete decomposition of the stable CH_4 molecule; only temperatures of 1400 °C and above ensure (near-complete) decomposition.[18,19]

Furthermore, C_2H_2 has been identified as a particularly important intermediate during hydrocarbon pyrolysis,[18] which explains its presence over almost the entire temperature range tested herein. The transient maximum of acetylene at 1400 °C likely reflects the accumulation of C_2 fragments under high-temperature, short-residence conditions, before further cracking and dehydrogenation convert them into H_2. This mechanistic interpretation is consistent with established radical-mediated chain- and β-scission pathways reported for PE and PP pyrolysis.[20–22] Also, the ethylene yield remained relatively stable between 900 °C and 1500 °C, which can likely be explained by the fact that ethylene is a precursor of graphite adducts;[23] as discussed in the following, graphite is one of the solid products forming during HDPE pyrolysis under these conditions.

When comparing the H_2 yield of 12.8 wt% observed during the experiment conducted at 1600 °C to the hydrogen mass fraction in HDPE of about 14.2 wt% reported by He *et al.*,[24] it is evident that during high-temperature pyrolysis a significant portion (around 90.1 wt%) of the hydrogen is released into the gas phase as molecular H_2. According to the principles of thermodynamics, it is expected that high temperatures maximize the yield of hydrogen or lead to the formation of solid, ordered structures such as graphite.[25] These trends align well with observations from previous studies on plastic pyrolysis conduced in our group in the same laboratory-scale setup employed herein: the same gaseous products were found during LDPE pyrolysis, with similar temperature-dependent trends as observed in the present study.[16] Other groups addressed the thermal pyrolysis of polyethylene as well; while the same gas phase species were identified, their levels vary, which we attribute to different reaction environments or reactor geometries. For instance, in line with our present findings, Scott *et al.*[26] report that the decomposition of LDPE increases with temperature, however, yielding higher amounts of ethylene and propylene at 700 °C. More importantly, Natesakhawat *et al.*[27] conducted pyrolysis experiments on HDPE at temperatures up to 900 °C. They report the highest H_2 yield at 900 °C, with ethylene as the main carbon product at 700 °C. Additionally, they observed a shift in product distribution toward higher cracked hydrocarbons at elevated temperatures, which supports the findings of this work material-wise; the main difference between LDPE and HDPE lies in the production-related higher proportion of side

chains.[28] LDPE is produced from ethylene under high pressure through a radical process, which allows for only little or no control over stereochemistry. This leads to a comparatively high proportion of side chains, resulting in a low crystallite content and low density. In contrast, HDPE is produced catalytically using the Ziegler–Natta process, which minimizes side chain formation and produces polymers with high crystallite content and high density. By integrating the findings from the present investigation with previously reported data on the pyrolysis of LDPE[16] it can be inferred that, for polymers exhibiting identical chemical composition and comparable molar masses, the influence of structural variations on the composition of gaseous pyrolysis products at elevated temperatures is minimal.

The influence of pressure was investigated in a subsequent series of tests conducted with an argon flow rate of 175 ml min^{-1}. Based on the previous experiments, a pyrolysis temperature of 1000 °C was selected, as this ensures both sufficient polymer conversion and the formation of a broad spectrum of gaseous products. This temperature thus provides an optimal basis for investigating the effects of pressure variation on the individual pyrolysis species.

Fig. 3 shows the results of the analysis of the gas phase products evolving when varying the pressure in the reactor between 0.1 and 0.5 MPa. While the hydrogen content in the product gas decreased slightly with increasing pressure, the methane content exhibited the opposite trend. Ethane, ethylene, and acetylene were detected only in low concentrations, and propylene was not detected at all.

Pressure-induced variations of the overall gas composition were found less pronounced than those related to temperature variations. As illustrated in Fig. 3a, an increase in pressure led to a slight reduction in hydrogen yield, whereas methane exhibited a local maximum between 0.2 and 0.3 MPa.

Although on a low absolute concentration level, acetylene yield shows a strong dependence on pressure. While it is formed with a yield of 0.6 wt% at 0.1 MPa, it cannot be detected above 0.3 MPa (Fig. 3b). Furthermore, no clear trend could be determined for ethane across the investigated pressure range. Notably, propylene was not detected under any of the applied pressure conditions. These observations suggest that within the range tested herein, pressure has only a limited effect on the formation of gaseous pyrolysis products, with methane showing the most significant variation. The observed minor decline in hydrogen concentration with increasing pressure implies a kinetically controlled reaction mechanism, which contrasts with expectations based on the thermodynamic equilibrium that would typically favor the formation of hydrogen and graphite.

Influence of temperature on the gas phase species evolving from PP pyrolysis

Fig. 4 shows the gas yield of the product gases from PP pyrolysis at temperatures from 800 to 1600 °C at a pressure of 1 bar. The hydrogen yield rises with temperature and reaches its maximum around 1200 °C. Above this

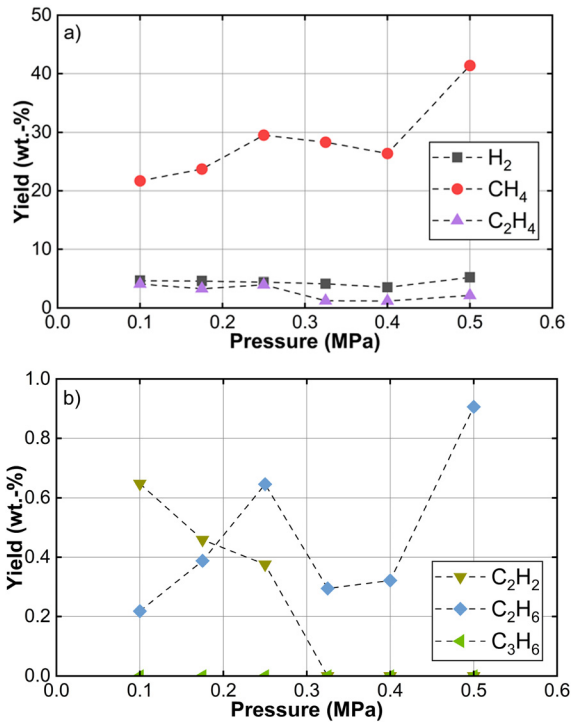

Fig. 3 Influence of pressure on the product gas composition from pyrolysis of HDPE at 1000 °C with yields of main (a) and minor (b) gaseous products.

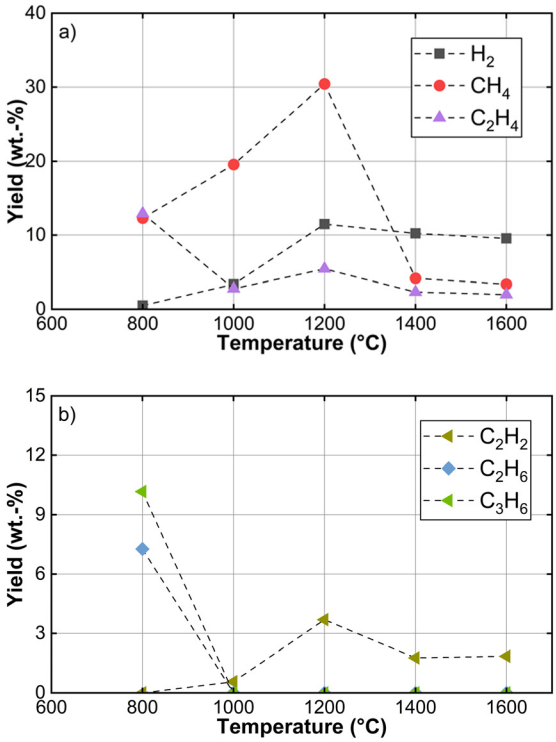

Fig. 4 Gas phase results of the PP pyrolysis with τ = 10 s at 1 bar. Temperature variation from 800 °C to 1600 °C with yields of main (a) and minor (b) gaseous products.

temperature, the yield decreases only slightly, making hydrogen the dominant product at high temperatures (≥1400 °C). In contrast, methane is the main gaseous product at lower temperatures. Its yield increases up to 1200 °C and then decreases significantly at higher temperatures. Ethylene shows a slight maximum at 1200 °C before declining again, whereas ethane and propylene were detected only at 800 °C. Small amounts of acetylene are formed at temperatures from 1000 °C to 1600 °C. The comparison of gas phase products from the pyrolysis of PP and HDPE reveals both similarities and distinct differences in product distribution and temperature dependency.

For both polymers, methane is the main hydrocarbon product at lower temperatures. In HDPE pyrolysis, methane reaches its methane yield continues to rise to 1200 °C before beginning to decline. This shift to higher temperatures for methane formation in PP pyrolysis suggests a different degradation behavior due to its polymer structure. Hydrogen formation increases continuously with temperature for both polymers, which aligns with findings obtained by Honus *et al.*[29]

Ethylene evolution from the two polymers strongly differs during pyrolysis: In HDPE pyrolysis, ethylene is the main product at lower temperatures, peaking around 800–900 °C with high yields; in contrast, PP pyrolysis generally yields lower amounts of ethylene. This reflects the different monomer structures, as ethylene is the repeating unit of HDPE but not of PP. Consequently, it is hardly surprising that propylene displays distinct behavior during PP pyrolysis. While propylene yields in HDPE are negligible across all temperatures, significant propylene formation occurs in PP pyrolysis at 800 °C, which quickly decreases and becomes undetectable above 1000 °C. Ethane is relevant only at low temperatures for both polymers but disappears at higher temperatures, with yields showing only minor differences. Acetylene forms in small amounts from both polymers, with yields peaking at intermediate temperatures. While the overall trends are similar, the maximum acetylene yield during PP pyrolysis is slightly higher and occurs at a higher temperature compared to HDPE. A similar trend was observed by Al-Salem *et al.*,[30] who found alkenes and alkanes (C_2–C_4) as main product gases during the pyrolysis of HDPE at temperatures ranging from 500 °C to 800 °C in a fixed bed reactor.

In summary, although HDPE and PP pyrolysis exhibit similar temperature-dependent trends, significant differences arise in the yields of ethylene and propylene due to their distinct monomer structures. PP demonstrated a delayed maximum for methane, higher hydrogen yields at elevated temperatures, and increased propylene formation at lower temperatures. These observations highlight the influence of the polymer structure on the pyrolysis behavior.

Influence of temperature on the gas phase species evolving from pyrolysis of a HDPE/PP mixture

Pyrolysis experiments involving a binary mixture of high-density polyethylene (HDPE) and polypropylene (PP) were performed under identical conditions to those applied to the individual polymers: the thermal degradation processes were carried out across a temperature range of 800 to 1600 °C at an atmospheric pressure of 1 bar. The gas phase analysis of the mixtures reveals product distributions that fall between the behaviors of the individual polymers, as illustrated in Fig. 5.

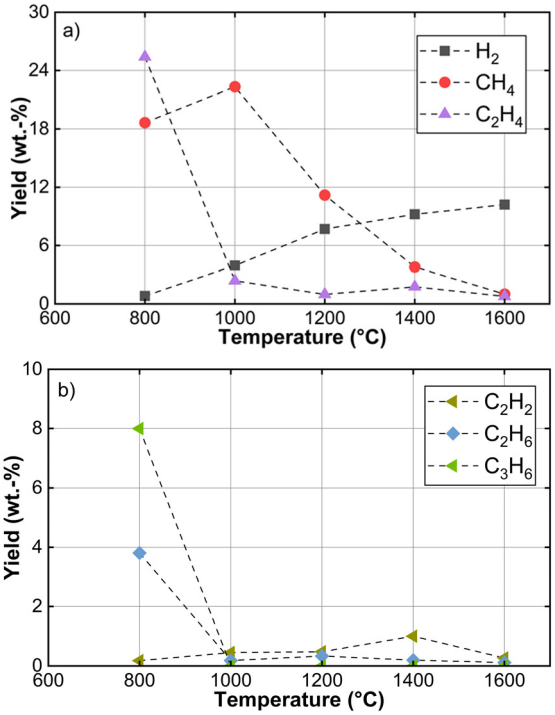

Fig. 5 Gas phase composition obtained from pyrolizing a 1 : 1 mixture of HDPE and PP with τ = 10 s at 1 bar. Temperature variation from 800 °C to 1600 °C with yields of main (a) and minor (b) gaseous products.

Methane remains the dominant hydrocarbon at lower temperatures, similar to pure PP. Its yield peaks around 1000–1200 °C, although the maximum yield is lower than that observed during pyrolysis of pure PP. Upon a further increase in temperature, the methane yield decreases continuously. This suggests that, in mixtures, the methane formation is influenced by both polymers, shifting the maximum yield toward an intermediate temperature. Hydrogen formation shows a steady increase with temperature, comparable to the data obtained during pyrolysis experiments with the pure polymer materials. However, the maximum hydrogen yield in the mixtures is slightly lower than in pure PP pyrolysis, yet still significantly higher than for HDPE. This underlines the dominant effect of PP on hydrogen production within the mixture. Ethylene is formed in moderate amounts at lower temperatures, with yields decreasing rapidly above 1000 °C. The behavior of ethylene strongly resembles that of pure PP rather than HDPE, although the yields are generally lower. Ethane and propylene are detectable only at lower temperatures and disappear at higher temperatures, consistent with the behavior observed for both pure polymers. Their yields are

slightly reduced compared to PP pyrolysis alone. Acetylene appears in small amounts, peaking around 1200 °C before decreasing again. The yield is slightly lower than in the experiments with pure PP, but the trend remains comparable.

It is important to note that the formation of acetylene contributes to soot formation and carbon deposition.[31] Overall, the pyrolysis of HDPE/PP mixtures results in product yields that lay between those of the individual polymers. Methane and hydrogen formation are mainly influenced by the PP content, while ethylene yields remain moderate due to the lack of clear dominance from either polymer. The results confirm that blending HDPE with PP alters the product distribution without generating entirely new product trends. It is also important to notice that the temperature ranges and main decomposition stages for HDPE, PP, and their mixtures (700–900 °C) align with mechanistic models that describe polyolefin pyrolysis as a radical-chain process driven by random scission, backbiting, and β-scission reactions.[32,33] The detailed HDPE decomposition model by Levin and Broadbelt[34] as well as the mechanistic frameworks developed by Ranzi *et al.*[35] for pyrolytic PE/PP decomposition indicate a shifting relevance from condensable hydrocarbons at lower temperatures to gaseous species as the temperature increases. The rising levels of H_2 and light gaseous products observed in the present work at temperatures of ≥900 °C support these predictions, suggesting an increased role of secondary gas phase cracking and dehydrogenation pathways. At ultra-high temperatures ranging from 1200 °C to 1600 °C, the gas phase analysis indicates a significant increase in H_2 yield. This is in line with existing studies on high-temperature pyrolysis of plastics, where rapid dehydrogenation, ring growth, and graphitization are prevalent, necessitating quenching to prevent recombination.[36] Additionally, the observed trend of higher gas yields from HDPE relative to PP in this temperature range agrees with reported pyrolysis data between 900 and 1100 °C, where HDPE produces more gaseous products than PP.

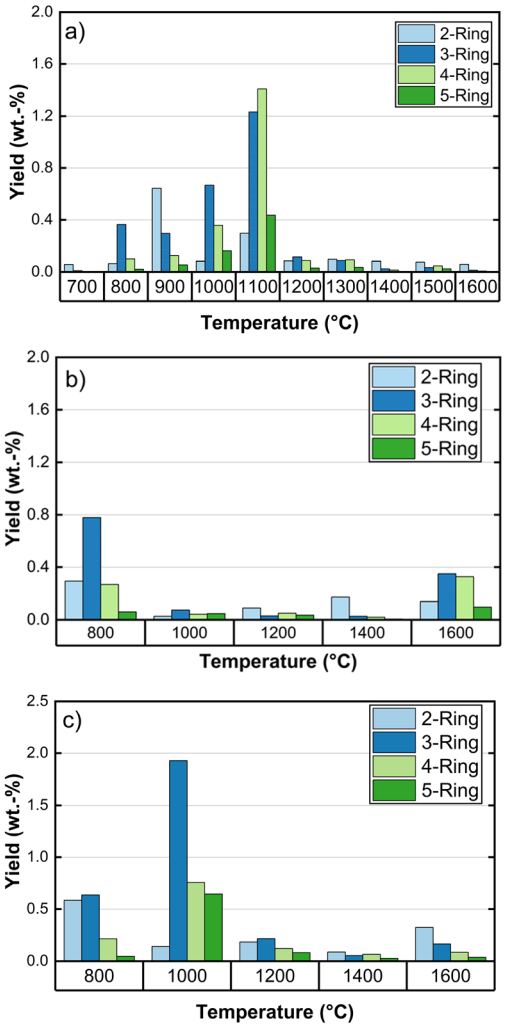

Fig. 6 Influence on the temperature on the condensed aromatic phase from pyrolysis of HDPE (a), PP (b), and a 1 : 1 mixture of HDPE and PP (c).

Liquid phase analysis

Aromatics. The analysis of aromatic fractions from the pyrolysis of HDPE, PP, and their 1 : 1 mixture reveals distinct formation patterns influenced by polymer type and reaction temperature as illustrated in Fig. 6. For HDPE, no clear temperature-dependent trend in the yield of polycyclic aromatic hydrocarbons (PAHs) could be established, as depicted in Fig. 6a.

Despite some variation was observed in the data, the results consistently showed that higher aromatic yields were achieved at higher temperatures, while changes in process conditions had minimal impact on the overall aromatic fraction. This trend is consistent with the findings of Natesakhawat *et al.* and Oravová *et al.*, who revealed that in the pyrolysis of HDPE, PAH amounts are minimal at lower temperatures but increase significantly once temperatures reach 700 °C and above, particularly under longer residence times due to enhanced cracking and condensation reactions.[27,37] A similar behavior was observed in this study, where the amount of PAHs rose progressively from 800 °C to 1100 °C, followed by a decline as the temperature was raised further from 1200 °C to 1600 °C.

In contrast, PP pyrolysis resulted in noticeably lower aromatic yields compared to HDPE. The highest yield of aromatics was observed at 800 °C, with yields declining sharply at higher temperatures due to its branched structure. The branched structure allows easier fragmentation, creates more aromatic precursors and thus greater PAH formation at lower temperatures.[38,39] This could also be an explanation for the 3-ring aromatic fraction that stands out at 800 °C. The HDPE/PP mixture displayed a combined behavior: at lower temperatures, the aromatic yields and product distribution closely resembled those of HDPE pyrolysis, with cumulative yields between 1.5 and 3.5 wt% and tricyclic aromatics dominating. However, at higher temperatures, aromatic

yields decreased significantly, aligning more closely with the trends observed in PP pyrolysis. Above 1000 °C, the formation of aromatics remained consistently low, with a balanced distribution of different aromatic classes. These observations suggest that both polymers contribute to PAH formation, however, the branched structure of PP offers more aromatic precursors, leading to a higher overall PAHs yield below 1000 °C and a suppression of aromatics formation at elevated temperatures (>1000 °C) compared to HDPE.

Previous kinetic studies comparing pyrolytic degradation of HDPE and PP show that PP decomposition requires a significantly lower activation energy and degrades more readily under thermal stress than HDPE.[20,21,40] In isothermal and non-isothermal pyrolysis experiments, PP generates predominantly light *n*-alkanes/alkenes and volatile products, with only minor contributions to heavy or polyaromatic condensates. Under the fast-heating and short residence-time conditions of our setup, such behavior could lead to a rapid backbone scission mechanism that hampers secondary reactions leading to large polyaromatic or coke-like products. This explanation also supports the previously mentioned enhanced 3-ring fraction at 800 °C for PP and at 1000 °C for the mixture. That the decomposition behavior of the mixture differs from the individual component degradation mechanisms is in line with previous studies by Netsch *et al.*[41] and Wu *et al.*,[42] which both indicate interactions between intermediates from two different plastics during their simultaneous degradation.

Moreover, the results of our study reveal an increase in PAH concentrations as the temperature rises from 800 °C to 1000 °C. This aligns with the findings of Oravová *et al.*,[37] who demonstrated that both the yield and complexity of PAHs significantly increase if temperatures exceed 700 °C. This phenomenon is attributed to enhanced secondary reactions at elevated temperatures, including the condensation and aromatization of smaller hydrocarbon fragments, which produce larger and more complex PAH molecules.[37,43]

In summary, HDPE promotes aromatic formation during pyrolysis, particularly at lower temperatures, while PP yields fewer aromatic products. In mixed-polymer systems, this leads to HDPE-like behavior at low temperatures and reduced aromatic formation at high temperatures.

Aliphatics. The analysis of aliphatic hydrocarbon fractions with high boiling temperatures, in the following referred to as high-boiling aliphatics, is presented in Fig. 7. The data did not reveal a clear trend regarding the overall yield of the aliphatic fraction formation from HDPE pyrolysis. It was observed that pyrolysis oil derived from the high-temperature pyrolysis of HDPE contains only a minor proportion of aliphatic components.

Within the individual fractions, there is a tendency for higher molecular weight fractions to increase with temperature. At 700 °C, the distribution of fractions is nearly uniform, with an average yield of 0.003 wt%. However, the C_{26}–C_{30} fraction significantly rises to 0.31 wt% at 1500 °C.

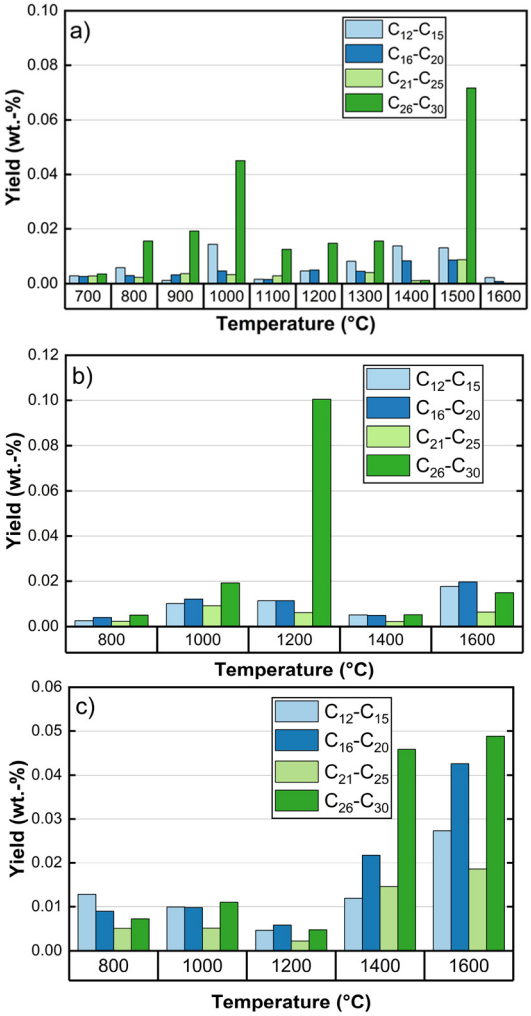

Fig. 7 Influence on the temperature on the condensed aliphatic phase from pyrolysis of HDPE (a), PP (b) and a 1 : 1 mixture of HDPE and PP (c).

Notably, yields of aliphatic compounds were negligible at 1600 °C. These observations suggest that the reaction at elevated temperatures is kinetically controlled, leading to high reaction rates and the formation of products that may not be the most thermodynamically stable species. Kinetic studies have shown that under fast, high-temperature pyrolysis conditions, the formation of highly reactive and short-lived intermediates and less stable products is favored because the limited residence time prevents equilibrium from being reached.[44,45]

The rapid pressure changes upon exposure of the plastics samples to the high temperatures indicate a fast decomposition reaction that goes along with gas formation, and it is possible that some reaction intermediates are expelled from the reactor before complete conversion occurs. Compared to LDPE pyrolysis, the overall yield of aliphatic compounds is significantly lower.[16]

To some extent, this discrepancy may stem from methodological variations, specifically the condensation method with varying cooling rates, which greatly affects the

recovery of low-boiling aliphatic products. Equally important, the intrinsic structure of the polymers plays a key role: LDPE's highly branched structure, with its high amount of side chains, likely produces more aliphatic compounds during thermal decomposition. In contrast, HDPE's mostly linear structure limits aliphatic formation, as the lack of branches reduces the pathway for side chains cleavage. Structural and methodological factors, including condensation efficiency and heating rate, lead to lower yields of aliphatic compounds in HDPE pyrolysis compared to LDPE.[46,47] For PP, the results similarly indicate generally low yields of aliphatic compounds, with cumulative amounts rarely exceeding 0.02 wt%. The highest total yield of 0.12 wt% stands out and was observed at 1200 °C, predominantly within the C_{26}–C_{30} fraction. Due to the rapid and variable behavior of the pyrolysis process, as well as the narrow occurrence of this peak, it cannot be conclusively attributed to a temperature effect. Instead, such yield may arise from the interaction of process parameters, such as argon residence time and pressure. At lower temperatures, particularly at 800 °C, yields remained below 0.02 wt%. No clear trend was established from the distribution of the chain lengths, indicating that aliphatic formation during PP pyrolysis may be less sensitive to temperature variations compared to HDPE. At lower temperatures, both PP and HDPE yield small amounts of aliphatic compounds. As the temperature rises, the fraction of straight-chain aliphatic compounds decreases for both polymers due to the promotion of thermal cracking reactions, leading to the formation of more cyclic and aromatic compounds.[38,48] However, the pyrolysis of PP tends to produce a greater amount of branched aliphatic compounds compared to HDPE, which generates a higher proportion of linear aliphatics at lower temperatures.

The HDPE/PP mixture exhibited distinct behavior. Although low total yields were recorded at temperatures up to 1200 °C, with a minimum of 0.02 wt% at that temperature, a pronounced increase in aliphatic product formation occurred at higher temperatures. At 1400 °C and 1600 °C, cumulative yields of 0.09 wt% and 0.14 wt% were measured, respectively. In contrast to the experiments with individual polymers, a shift towards higher molecular weight fractions (specifically C_{26}–C_{30}) was observed at these elevated temperatures. This trend was consistently reproduced across multiple experimental runs, indicating a systematic and reproducible effect on aliphatic formation at high temperatures attributable to the polymer mixture. The data suggest that the combination of HDPE and PP promotes the generation of long-chain aliphatic hydrocarbons during high-temperature pyrolysis, potentially due to intermolecular interactions between the degradation intermediates of both polymers during their co-pyrolysis.[48,49] In summary, while the pyrolysis of HDPE and PP individually yields low amounts of aliphatic products with no clear temperature dependence, the co-pyrolysis of the polymer mixture demonstrates a temperature-dependent increase in aliphatic yield, particularly for heavier fractions. These observations underscore the significant role of polymer–polymer interactions in modulating the product distribution during mixed-plastic pyrolysis. For designing real-world PW pyrolysis processes, these findings are of particular significance, as they allow either the plastics to be specifically engineered or, given that PW is typically a combination of different plastics, the process conditions like temperature needs to be adjusted so that pyrolysis produces a lower fraction of aliphatic compounds.

Characterization of the carbonaceous solid phase

Beyond a mere analysis of gas phase products as well as aromatic and aliphatic products, the structure of the carbonaceous solid product was analyzed as well. In particular, the carbon accruing during pyrolysis experiments conducted at temperatures of 1200 °C, 1400 °C, and 1600 °C

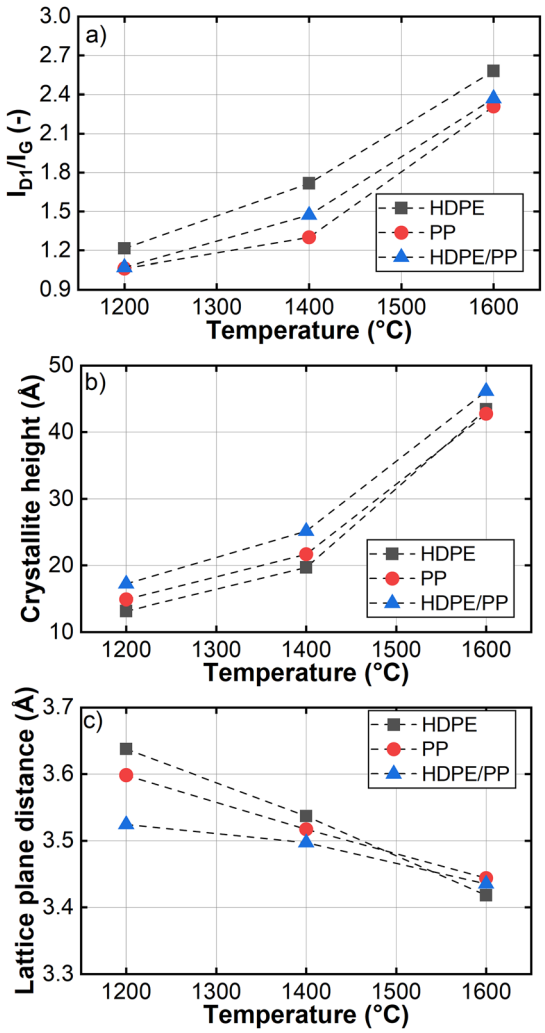

Fig. 8 The I_{D1}/I_G band ratio according to the Raman results (a) as well as crystallite height (b) and lattice plane distance (c) according to the XRD data.

for HDPE, PP, and their 1 : 1 mixture was characterized using Raman spectroscopy and X-ray diffraction (XRD).

Fig. 8 summarizes the findings. Raman spectra and X-ray diffraction patterns can be found in Fig. S2 and S3 in the SI. Fig. 8a shows the ratio of the I_{D1} and I_G bands from the Raman spectra obtained for the carbonaceous residues. These specific bands were chosen for analysis because previous research identified their ratio as a reliable descriptor of the graphitization degree.[50,51] The I_G band represents the ordered carbon structure, while the I_{D1} band indicates defects within that structure. This makes their intensity ratio an excellent indicator of the material's structural ordering. For the pyrolysis experiments conducted herein, the evaluation of the Raman spectra revealed that the I_{D1}/I_G ratio increases with increasing pyrolysis temperature, suggesting more defect formation at higher temperatures across all samples. For HDPE, the I_{D1}/I_G ratio increased from 1.2 at 1200 °C to 2.3 at 1600 °C. This increase suggests that higher temperatures promote defect formation rather than optimal graphitic ordering. Intensity fluctuations observed in the Raman spectra were attributed to sample inhomogeneities, limiting further interpretation. PP exhibited a similar temperature-dependent increase but had slightly lower initial values for the I_{D1}/I_G ratio. The results suggest that, compared to HDPE, at lower temperatures the branched molecular structure of PP facilitates the formation of more graphitic domains during pyrolysis. The pyrolysis of the HDPE/PP mixture results in carbonaceous products with defect density between those of the pure polymers but closely resembling the PP behavior. This indicates a strong influence of PP on the graphitic structure formation in the blend, promoting less defect formation at lower to intermediate temperatures. The increasing trend of I_{D1}/I_G ratio with temperature remained consistent. Overall, these data indicate an increasing defect density and kinetic hindrance to graphitization at elevated temperatures. Similar trends in the evolution of carbon structure with pyrolysis temperature have also been observed in PET-derived carbon materials, where Raman analyses indicate changes in defect density of pyrolytic carbon with increasing temperature.[52]

The conclusions drawn from the Raman spectra are complemented by the X-ray diffraction patterns that allow to quantify crystallite size and interlayer spacing. For HDPE-derived carbon, crystallite heights increased from 13.13 Å at 1200 °C to 43.39 Å at 1600 °C (Fig. 8b), while interlayer spacing (d_{002}) decreased from 3.64 Å to 3.42 Å (Fig. 8c). These results point to the growth of larger and more structurally ordered graphitic crystallites with increasing temperature. This trend is concurrent to the Raman results that point to an increase in defect structures, which suggests a complex interplay between crystallite growth and defect generation mechanism. PP exhibited larger crystallites at all temperatures, starting at 17.21 Å at 1200 °C and reaching 42.74 Å at 1600 °C, with slightly smaller interlayer spacings compared to HDPE. This corroborates the Raman observation of enhanced graphitization, reflecting easier crystallite growth facilitated by PP's molecular architecture. Pyrolysis of the HDPE/PP mixture yielded the largest crystallites at 1200 °C and 1400 °C, measuring 17.21 Å and 25.13 Å, respectively, thus surpassing both pure polymers; the corresponding interlayer spacings for the mixture-derived carbon were 3.53 Å and 3.50 Å, respectively. At 1600 °C, crystallite size (46.14 Å) and spacing (3.44 Å) converged to values comparable to those of the individual polymers. This non-linear enhancement suggests synergistic interactions during pyrolysis that promote superior graphitic ordering and crystallite growth at moderate temperatures in the blend. Furthermore, the results imply that the smaller crystals formed at lower temperatures exhibit a high degree of disorder. Comparatively, the relatively large distance between atomic layers further supports this finding. For example, Bacon reported a lattice plane spacing of 3.35 Å for highly ordered graphite, which increases with a greater degree of disorder.[53]

In conclusion, the pyrolysis temperature significantly influences the development of carbon structures in all samples. Graphitization decreases with increasing temperature due to kinetic limitations and defect formation. PP consistently forms more ordered graphitic structures at lower temperatures than HDPE, as evidenced by higher graphitization degrees and larger crystallites. The HDPE/PP mixture exhibits a synergistic effect, enhancing graphitic ordering and crystallite growth beyond the simple averaging of the pure components, especially between 1200 °C and 1400 °C. At 1600 °C, thermal effects dominate, resulting in smaller polymer-specific influences and leading to converging carbon structural characteristics across all samples. Such a detailed knowledge of the material properties is of major importance, as these characteristics determine usage options and functional performance of the accruing carbonaceous solid residues. For instance, carbon with a high degree of graphitization can be used for conductive additives or anodes in battery application, as a higher degree of graphitization can be linked to higher capacity. Prior to implementation into actual applications, further parameters such as specific surface area or particle size need to be investigated. It should be noted that the counter-intuitive trend revealed by analysis of the Raman spectra – decreasing graphitization upon higher pyrolysis temperature – may be caused by the relatively short duration of our experiments. The higher structural order of the high-temperature samples on the level of crystallites may suggest an incomplete phase transformation of the solid, which initiates on a microscopic scale, but did not extend to the macroscopic scale. Thus, a longer exposure of carbonaceous residues to high temperatures is expected to enable higher graphitization degrees, similar to the thermal treatment of carbon commonly employed for graphite production.[54–56]

Furthermore, it is important to note that intermediates composed of aliphatic and polycyclic aromatic hydrocarbons could have influence on the Raman spectra, as reported by Sadezky *et al.*[57] Finally, it is important to highlight that only crystalline structures contribute to the patterns in X-ray

diffraction, while Raman spectra are generally derived from molecular vibrations. Raman spectroscopy extends insights gained by XRD by identifying both ordered and disordered structures, providing a more comprehensive understanding of the carbonaceous solids. This included insights into defects, disorder, and molecular bonding that do not generate diffraction peaks. The pyrolysis temperature significantly influences the properties of carbon generated from the pyrolysis of HDPE, PP and the mixture HDPE/PP. Elevated temperatures resulted in smaller particle sizes, unique crystallite structure, and reduced graphitization degree. These findings enhance the understanding of the mechanisms involved in carbon formation during the plastic wastes pyrolysis.

Conclusion

The thermal pyrolysis behavior of HDPE, PP, and their mixture was investigated through high-temperature experiments in a laboratory-scale reactor. Gaseous, liquid, and solid products were analyzed using gas chromatography for gaseous and liquid phases, and Raman spectroscopy as well as X-ray diffraction (XRD) for solid residues. Especially the nature of gas phase products was found to be strongly governed by temperature: While at temperatures between 700 °C and 1000 °C the product gas primarily comprised methane and ethylene, a further temperature increase promoted hydrogen evolution, with maximum hydrogen yields of 12.8 wt% for HDPE, 11.5 wt% for PP, and 10.2 wt% for HDPE/PP. Furthermore, the aromatic content in the liquid phase increased with temperature, especially for PP and the HDPE/PP mixture, indicating enhanced secondary reactions and cyclization. In contrast, HDPE pyrolysis yielded a higher proportion of aliphatic hydrocarbons, reflecting its linear polymer structure and a reduced tendency to undergo aromatization. The mixture exhibited intermediate behavior, with PP predominantly influencing gas phase composition at high temperatures. As the pyrolysis temperature increased, liquid yields generally decreased due to an enhanced conversion of aromatic and aliphatic compounds into gaseous species and solid residues. The aromatic content in the condensate increased, especially for the PP and mixed samples, which correlates with the increased gas phase aromatics and indicates thermal cracking and dehydrogenation; liquids derived from HDPE remained more saturated and aliphatic in character.

The Raman spectra of the solid carbonaceous residues revealed a consistent decrease in the graphitization degree with increasing temperature for all samples, attributed to the formation of defect-rich, disordered carbon structures due to kinetic limitations at elevated temperatures. Carbon obtained during PP pyrolysis showed the highest initial graphitization degree, followed by the HDPE/PP mixture, and then HDPE. Furthermore, XRD revealed increasing crystallite size and decreasing interlayer spacing, reflecting the growth of ordered graphitic domains. This apparent discrepancy arises from the differing sensitivities of the techniques, with XRD detecting only crystalline domains, whereas Raman captures both ordered (crystalline) and disordered (amorphous or defect-rich) carbon structures. The HDPE/PP mixture exhibited synergistic effects, with PP enhancing graphitic ordering and producing larger crystallites at 1200–1400 °C. At 1600 °C, the differences between the samples diminished, pointing out a universal regime where thermal energy dominates over compositional effects.

Overall, hydrogen yields exceeding 12 wt% while producing solid carbon with properties attractive for utilization in rubber industry makes the pyrolysis of plastics an auspicious approach for waste utilization. During process design it is important to consider that the pyrolysis behavior depends strongly on the polymer type: as shown herein, PP favors aromatic compounds and highly graphitized solid carbon, whereas HDPE pyrolysis produces more aliphatic products; the HDPE/PP mixture inherits PP's beneficial structural traits in the solid phase. These results highlight the importance of feedstock composition and temperature for product distribution and carbon structure, and suggest further exploration of extended residence times, alternative reactors, and other plastics such as PS and PET to improve hydrogen production and plastic waste management.

Author contributions

V. M. Pohl: investigation, methodology, writing – original draft, validation, data curation, visualization, formal analysis. C. K. Fonzeu Monguen: investigation, methodology, writing – original draft, validation, data curation, formal analysis. D. J. Heitlinger: investigation, methodology, data curation, formal analysis. P. Lott: conceptualization, validation, writing – review & editing, supervision, project administration. O. Deutschmann: conceptualization, validation, writing – review & editing, supervision, resources.

Conflicts of interest

There are no conflicts to declare.

Data availability

The data used in this study are summarized in the figures and tables of the paper and in the SI. Raw data are available upon reasonable request from the corresponding author. Supplementary information is available. See DOI: https://doi.org/10.1039/d5re00442j.

Acknowledgements

We thank M. Berg and C. Kroll (Berg-idl GmbH) for their support in engineering the high-temperature vessel of the experimental setup, and S. Lichtenberg and Felix Straub (both KIT) for technical support. The authors thank H. Müller, L. Baumgarten and A. De Giacinto, (all KIT) for scientific exchange and support in solid carbon analysis.

References

1 Plastics – the fast Facts 2024 • Plastics Europe, https://plasticseurope.org/knowledge-hub/plastics-the-fast-facts-2024/, (accessed 14 June 2025).
2 M. Sogancioglu, E. Yel and G. Ahmetli, *J. Cleaner Prod.*, 2017, **165**, 369–381.
3 F. Riedewald, J. Zuber, P. Rathsack, G. Duffy, M. O'Mahoney and M. Sousa-Gallagher, *Chem. Ing. Tech.*, 2023, **95**, 1332–1338.
4 I. A. Al-Khatib, J. Guo, K. Kuchta, A. A. Draidi, S. Y. Abu Amara and A. Alassali, *Sustainability*, 2023, **15**, 14640.
5 V. P. Ranjan and S. Goel, *Resour., Conserv. Recycl.*, 2021, **169**, 105494.
6 N. Zhao, S. S. Low, C. L. Law, T. Wu and C. H. Pang, *Fuel Process. Technol.*, 2025, **274**, 108239.
7 Council of the European Union, Council Directive 1999/31/EC of 26 April 1999 on the landfill of waste (consolidated text).
8 M. Solis and S. Silveira, *Waste Manage.*, 2020, **105**, 128–138.
9 A. Çelik, I. Ben Othman, Y. Neudeck, O. Deutschmann and P. Lott, *Energy Convers. Manage.*, 2025, **326**, 119414.
10 A. R. Hendrawati, M. Liandi, M. H. Solehah, I. Aziz Setyono and Y. D. I. Siregar, *Case Stud. Chem. Environ. Eng.*, 2023, **7**, 100290.
11 S. L. Wong, S. Armenise, B. B. Nyakuma, A. Bogush, S. Towers, C. H. Lee, K. Y. Wong, T. H. Lee, E. Rebrov and M. Muñoz, *J. Anal. Appl. Pyrolysis*, 2023, **169**, 105793.
12 K. Sivagami, K. V. Kumar, P. Tamizhdurai, D. Govindarajan, M. Kumar and I. Nambi, *RSC Adv.*, 2022, **12**, 7612–7620.
13 S.-M. Lee, S.-H. Lee and J.-S. Roh, *Crystals*, 2021, **11**, 153.
14 P. Lott, M. B. Mokashi, H. Müller, D. J. Heitlinger, S. Lichtenberg, A. B. Shirsath, C. Janzer, S. Tischer, L. Maier and O. Deutschmann, *ChemSusChem*, 2023, **16**, e202201720.
15 S. D. Angeli, S. Gossler, S. Lichtenberg, G. Kass, A. K. Agrawal, M. Valerius, K. P. Kinzel and O. Deutschmann, *Angew. Chem.*, 2021, **60**, 11852–11857.
16 C. K. F. Monguen, A. Çelik, F. Straub, V. Pohl, J. Kühn, P. Lott and O. Deutschmann, *J. Anal. Appl. Pyrolysis*, 2025, 107289.
17 A. Çelik, A. B. Shirsath, M. Mokashi, J. Tatzig, H. Müller, O. Deutschmann and P. Lott, *Chem. Eng. J.*, 2025, **515**, 163167.
18 M. Mokashi, A. Bhimrao Shirsath, P. Lott, H. Müller, S. Tischer, L. Maier and O. Deutschmann, *Chem. Eng. J.*, 2024, **479**, 147556.
19 A. Çelik, A. B. Shirsath, F. Syla, H. Müller, P. Lott and O. Deutschmann, *J. Anal. Appl. Pyrolysis*, 2024, **181**, 106628.
20 H. Bockhorn, A. Hornung, U. Hornung and D. Schawaller, *J. Anal. Appl. Pyrolysis*, 1999, **48**, 93–109.
21 A. Aboulkas, K. El harfi and A. El Bouadili, *Energy Convers. Manage.*, 2010, **51**, 1363–1369.
22 S. Natesakhawat, J. Weidman, S. Garcia, N. C. Means and P. Wang, *J. Energy Inst.*, 2024, **116**, 101738.
23 E. O. Pentsak, M. S. Murga and V. P. Ananikov, *ACS Earth Space Chem.*, 2024, **8**, 798–856.
24 T. He, C. Tong, L. Chen, Y. Zhou, B. Jin and B. Zhang, *Fuel*, 2021, **303**, 121231.
25 H. von Helmholtz, *Sitzungsberichte der Königlich Preussischen Akademie der Wissenschaften zu Berlin*, 1882, 22–39.
26 D. S. Scott, S. R. Czernik, J. Piskorz and D. S. A. G. Radlein, *Energy Fuels*, 1990, **4**, 407–411.
27 S. Natesakhawat, J. Weidman, S. Garcia, N. C. Means and P. Wang, *J. Energy Inst.*, 2024, **116**, 101738.
28 G. Odian, *Principles of Polymerization*, John Wiley & Sons, 2004.
29 S. Honus, S. Kumagai, G. Fedorko, V. Molnár and T. Yoshioka, *Fuel*, 2018, **221**, 346–360.
30 S. M. Al-Salem, *Process Saf. Environ. Prot.*, 2019, **127**, 171–179.
31 A. B. Shirsath, M. Mokashi, P. Lott, H. Müller, R. Pashminehazar, T. Sheppard, S. Tischer, L. Maier, J.-D. Grunwaldt and O. Deutschmann, *J. Phys. Chem. A*, 2023, **127**, 2136–2147.
32 A. Locaspi, A. Frassoldati and T. Faravelli, *Chem. Eng. J.*, 2024, **500**, 156949.
33 Y. Zhang, Z. Fu, W. Wang, G. Ji, M. Zhao and A. Li, *ACS Sustainable Chem. Eng.*, 2022, **10**, 91–103.
34 S. Natesakhawat, J. Weidman, S. Garcia, N. C. Means and P. Wang, *J. Energy Inst.*, 2024, **116**, 101738.
35 E. Ranzi, M. Dente, T. Faravelli, G. Bozzano, S. Fabini, R. Nava, V. Cozzani and L. Tognotti, *J. Anal. Appl. Pyrolysis*, 1997, **40–41**, 305–319.
36 Y. Du, B. Solène, P. Glarborg and H. Wu, *Fuel*, 2024, **361**, 130664.
37 L. Oravová, J. Snow, J. Tolaszová, D. Pilnaj, P. Midula, J. Ševčíková and P. Kuráň, *Ecol. Eng. Environ. Tech.*, 2024, **25**, 256–264.
38 I. Dubdub and M. Al-Yaari, *Materials*, 2020, **13**, 4912.
39 E. Esmizadeh, C. Tzoganakis and T. H. Mekonnen, *Polymers*, 2020, **12**, 1627.
40 R. A. A. Nugroho, A. F. Alhikami and W.-C. Wang, *Energy*, 2023, **277**, 127707.
41 N. Netsch, L. Schröder, M. Zeller, I. Neugber, D. Merz, C. O. Klein, S. Tavakkol and D. Stapf, *J. Therm. Anal. Calorim.*, 2025, **150**, 211–229.
42 J. Wu, Z. Jiang, V. S. Cecon, G. Curtzwiler, K. Vorst, M. Mavrikakis and G. W. Huber, *Green Chem.*, 2024, **26**, 11908–11923.
43 S. Natesakhawat, J. Weidman, S. Garcia, N. C. Means and P. Wang, *J. Energy Inst.*, 2024, **116**, 101738.
44 S. M. Al-Salem, *Process Saf. Environ. Prot.*, 2019, **127**, 171–179.
45 H. Li, O. Mašek, A. Harper and R. Ocone, *Can. J. Chem. Eng.*, 2021, **99**, 1733–1744.
46 I. Mastalski, N. Sidhu, A. Zolghadr, S. Maduskar, B. Patel, S. Uppili, T. Go, Z. Wang, M. Neurock and P. J. Dauenhauer, *Chem. Mater.*, 2023, **35**, 3628–3639.
47 P. Sudalaimuthu, U. Ali and R. Sathyamurthy, *Sci. Rep.*, 2024, **14**, 28442.
48 W. Wijayanti, M. Musyaroh and M. N. Sasongko, *J. Sustain. Dev. Energy Water Environ. Syst.*, 2022, **10**, 1–18.
49 Y. Misra, D. J. Prasanna Kumar, R. K. Mishra, V. Kumar and N. Dwivedi, *Water-Energy Nexus*, 2025, **8**, 55–72.

50 C. Lan, Y. Tang, X. Huan and Q. Che, *ChemistrySelect*, 2019, **4**, 5937–5944.
51 G. A. Barberes, D. A. L. Almeida, F. C. Marques, J. F. Alves, P. H. M. Toledo, R. de Oliveira, L. F. Maia, L. P. F. Peixoto, A. C. Sant'Ana, C. M. S. Izumi, G. F. S. Andrade, D. C. Dias Filho, T. R. Menezes, D. M. Ibanez and L. F. C. de Oliveira, *J. Raman Spectrosc.*, 2025, **56**, 1203–1214.
52 K.-H. Ko, T.-J. Park, V. Sahajwalla and A. Rawal, *Fuel*, 2021, **291**, 120153.
53 G. Bacon, *Acta Crystallogr.*, 1951, **4**, 558–561.
54 X. Xu, D. Cao, Y. Wei, A. Wang, G. Chen, T. Wang, G. Wang and X. Chen, *ACS Omega*, 2024, **9**, 2443–2456.
55 S.-H. Lee, Y.-M. Hwang, T.-S. Byun, J.-H. Ko and J.-S. Roh, *Carbon*, 2023, **208**, 443–451.
56 J. Wang, L. Kong, J. Bai, H. Li, Z. Bai, X. Li and W. Li, *Fuel*, 2018, **234**, 1173–1180.
57 A. Sadezky, H. Muckenhuber, H. Grothe, R. Niessner and U. Pöschl, *Carbon*, 2005, **43**, 1731–1742.